An analysis of the structure of laminar separation bubbles in swept infinite geometries

T. Hetsch [a,*], U. Rist [b]

[a] *Aircraft Research Association Ltd, Manton Lane, Bedford, MK41 7PF, UK*
[b] *Institut für Aerodynamik und Gasdynamik, Universität Stuttgart, Pfaffenwaldring 21, 70550 Stuttgart, Germany*

ARTICLE INFO

ABSTRACT

The influence of sweep on the general structure of short separation bubbles in strictly laminar flow fields on swept infinite geometries is investigated by theoretical analysis and direct numerical simulations (DNS). In this situation the 'independence principle' of the Navier–Stokes equations for incompressible flow enforces a unique topology for the mean flow, which includes the much better understood unswept separation bubbles as a special case: swept laminar separation bubbles form leading edge parallel streamtubes with a spanwise outflow and a helical motion inside directed parallel to the separation line. If chordwise inflow conditions are kept constant, their cross-sections stay independent of a rising sweep angle, as the spanwise velocity field is then merely superimposed over the unchanged flow of the corresponding unswept case. Their mean flow field follows strict scaling rules that may be derived analytically from the generic 45°-solution, as confirmed by DNS-results for a series of pressure-induced separation bubbles subjected to a systematic variation of the sweep angle between 0° and 60°.

1. Introduction

Due to strong adverse pressure gradients and moderate Reynolds numbers, separation bubbles are frequently encountered with high-lift devices, near the leading edges of thin profiles, on turbine blades of low-pressure gas turbines, blades of wind turbines or in the midsection of laminar airfoils for gliders. Important features of this phenomenon are illustrated in Fig. 1(a): A laminar boundary layer over a solid surface separates from the wall when subjected to a strong adverse pressure gradient. Below the highly unstable, separated shear layer a slow backflow, the so-called 'dead air region', is observed giving rise to the characteristic pressure plateau in the front part of the bubble. Boundary layer disturbances are strongly amplified in the shear layer which usually leads to a rapid laminar–turbulent transition. The more energetic turbulent boundary layer may then reattach to form a *transitional* separation bubble. In this case the steady description of Fig. 1(a) exists only in a time-averaged sense. Instead, simulations or photographs from experiments show a shear layer roll-up in the rear part of the bubble, which leads to periodic vortex shedding.

In very quiet environments laminar reattachment may alternatively occur due to a change in the surface geometry or the pressure gradient giving rise to *laminar* separation bubbles with periodic vortex shedding. If the general disturbance level of the inflow

is decreased further, the shedding ceases and the resulting separation bubbles become completely steady as in Fig. 1(b) or in the direct numerical simulation (DNS) of Briley [5]. Experimental realisations of steady and unsteady laminar separation bubbles were obtained by Bao [3] in a water towing tunnel behind a rounded backward facing step. Note that laminar and transitional separation bubbles are often not distinguished in the literature and simply referred to as 'laminar separation bubbles' as opposed to 'turbulent separation bubbles', which separate in a turbulent flow field.

Investigations of separation bubbles are rather challenging as complex, interacting phenomena as flow separation and reattachment, backflow, laminar–turbulent transition and vortex shedding occur. Therefore, research efforts so far have almost exclusively addressed the unswept case, which does not exhibit crossflow influences or the sweep angle as an additional parameter and is easier to realise in experiments and simulations. The reader may wish to refer to more recent publications as Spalart and Coleman [26], Spalart and Strelets [27], Alam and Sandham [1], Marxen, Lang, Rist and Wagner [21], Herbst and Henningson [10] or Jones, Sandberg and Sandham [17] and cited literature therein to get an overview over current research activities in connection with the DNS of unswept separation bubbles.

However, separation bubbles naturally appear in swept configurations for important technical applications, as the transitional separation bubble detected by Greff [9] on the slat of an Airbus A310 in landing configuration. Despite this, investigations about swept separation bubbles are still very rare: An extensive body of experimental data devoted to swept separation bubbles was pub-

---

* Corresponding author.
E-mail address: thetsch@ara.co.uk (T. Hetsch).
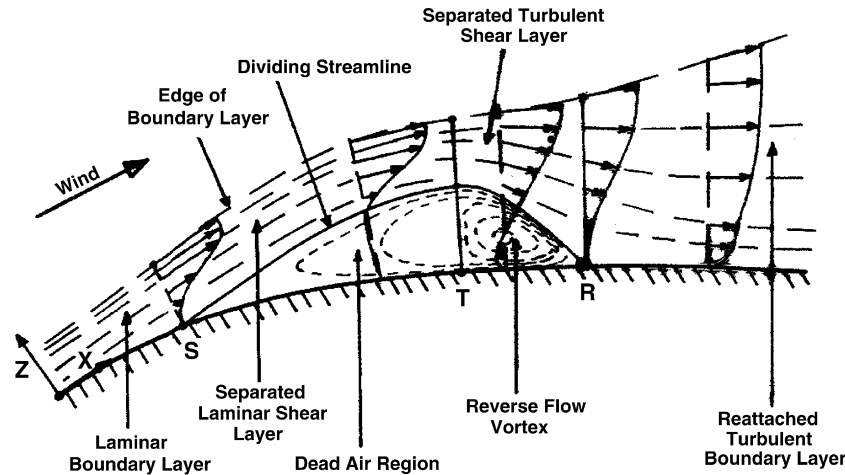
(a) Mean flow structure of a short, unswept transitional separation bubble after Horton (Fig. 2 in [15]). Separation of the laminar boundary layer at S, turbulent reattachment at R, idealised point transition in between at T. By courtesy of Dr. Horton.
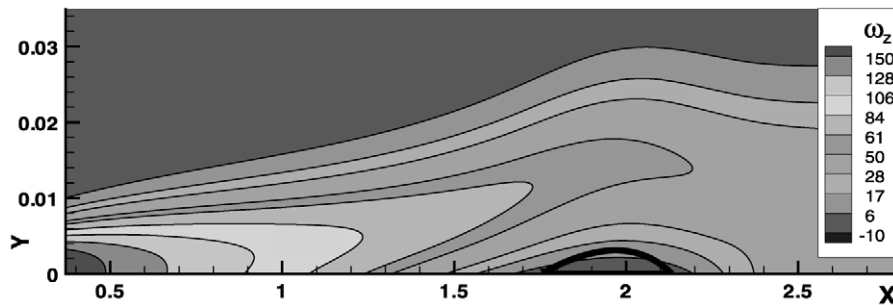
(b) Sweep angle $\Psi_\infty = 30°$ at $U_\infty = 30$ m/s, isolines of spanwise vorticity ω_z: Cross-section through a swept, stationary laminar separation bubble of the present DNS-base-flow without disturbance excitation. Visualised: Separated shear layer and dividing streamline. $Re_{\delta_2}(x_{\mathrm{sep}}) = 330$, based on the momentum thickness at separation.

Fig. 1. Basic properties of laminar and transitional separation bubbles. Unlike transitional bubbles laminar separation bubbles reattach in a still laminar flow regime, but show otherwise the same general structure.

lished by Young and Horton [29] and Horton [15] in the late 1960s, who investigated series of unswept and swept transitional separation bubbles through hotwire measurements in order to extend his semi-empirical theory for the prediction of the growth and bursting of bubbles to the swept case. Important flow parameters for a fixed sweep angle of 26.5° coincided with the unswept case if evaluated normal to the leading edge and not in the direction of the potential flow. Barkey-Wolfe [6] studied transitional separation bubbles on a flat plate behind different types of blunt leading edges for sweep angles between 0° and 45° experimentally. In particular he confirmed the independence of the mean reattachment position from the sweep angle. Selby [25] proved through systematic experimental investigations of *turbulent* separation bubbles behind backward facing steps that the mean reattachment position is independent up to about 38° depending on the step height. On the numerical side Davis, Carter and Reshotko [8] compared results from a compressible boundary layer code against one of Horton's separation bubbles, finding very good agreement for the pressure and the wall friction distributions. More recently, Kaltenbach and Janke [20], Kaltenbach [19] and Jürgens and Kaltenbach [18] studied sweep angle effects on the flow field behind a rearward-facing step, a geometry which naturally leads to a separation bubble immediately after the step, by means of large-eddy simulations and DNS.

As our knowledge about swept separation bubbles is still quite limited, the question arises how strongly they differ from the much better understood unswept case and to what degree results for the latter might be extendable to swept configurations. As far as the influence of sweep on their mean structure in strictly laminar flow fields in swept infinite geometries is concerned, a consequent ap-

plication of the so-called *independence principle* results in a unique topology which includes unswept bubbles as a special case. The independence of the streamwise quantities from the spanwise ones in flows which are homogeneous in span was first noted by Prandtl in the 1940s for the three-dimensional boundary layer equations and will be known to the reader in form of the Falkner–Scan profiles. Even for the swept case these two-dimensional velocity profiles remain unchanged or "independent" from the spanwise Cooke profile. Our aim is to demonstrate that the independence principle constitutes the key for the understanding of the general structure of laminar separation bubbles on configurations as for example swept infinite wings.

Thus the paper is organised as follows:

- Section 2 introduces general aspects of the independence principle and derives it from the governing equations as a basis for its subsequent application to laminar separation bubbles.
- Section 3 discusses to the numerical aspects of the study. The utilised DNS-algorithm is described and validated in Sections 3.1 and 3.2, respectively.
- Section 4 contains the main results: At first Section 4.1 focuses on the influence of sweep on the laminar flow quantities and general scaling laws are obtained. Afterwards a modified solution strategy for series of DNS-calculations with different sweep angles based on the independence principle is proposed in Section 4.2. It is transferable to arbitrary laminar flow fields on swept infinite geometries and results in considerable run-time savings. Finally, Section 4.3 applies the independence principle to swept laminar separation bubbles and discusses the resulting topology in detail.
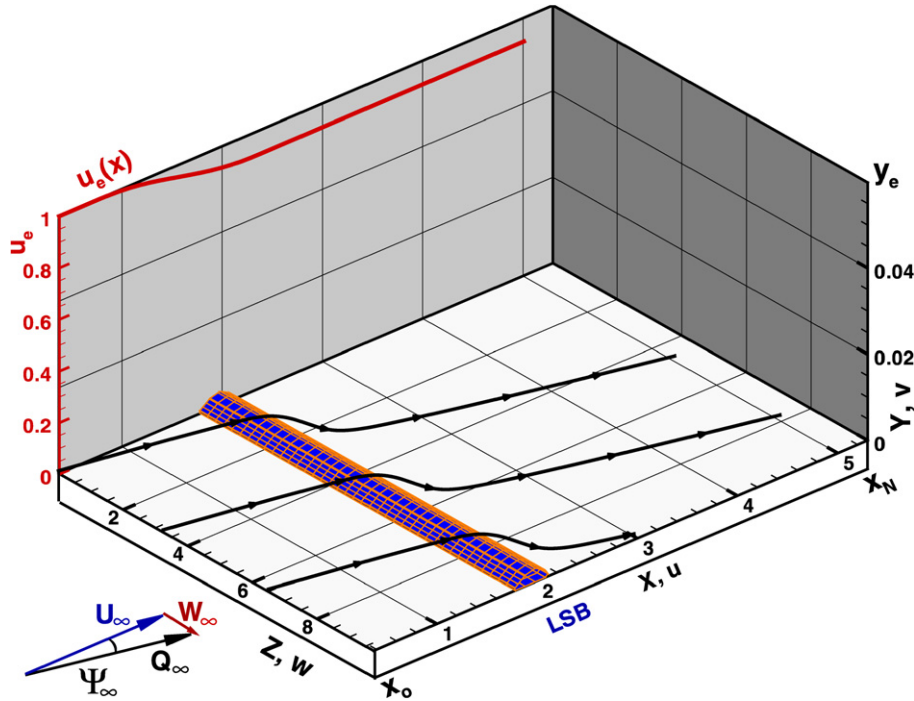
Fig. 2. Calculation domain of 30°-laminar separation bubble ($x \in [1.75; 2.13]$) with near-wall streamlines over dividing surface $\Psi_o = \{(x, y) \mid \Psi(x, y) = 0\}$. Oncoming flow: Sweep angle Ψ_∞ and inflow velocity Q_∞ with components U_∞ and W_∞. Prescribed upper boundary condition $u_e(x)$: Velocity distribution of potential flow. The domain extends from $x_o = 0.37$ to $x_N = 5.05$ in chordwise and from $y = 0$ to $y_e = 0.059 = 18 \cdot \delta_1(x_o)$ in wall-normal direction.

- The paper ends with a summary and the main conclusions in Section 5.

The presented simulations have been utilised as base flows by the authors in [11] and [12] for unsteady DNS investigating the interaction of oblique Tollmien–Schlichting waves with swept laminar separation bubbles. Additionally, these base flows were used to assess the principle applicability and the accuracy of spatial linear stability theory (LST) and solutions of the parabolised stability equations (PSE) in swept separation bubbles in [13]. Based on that, the influence of sweep on the linear stability of the present separation bubble series was analysed in Hetsch and Rist [14].

2. The governing equations and the independence principle for laminar flow

The present study is based on the three-dimensional, incompressible Navier–Stokes equations in a velocity–vorticity formulation. It can be derived from the classical formulation with the continuity equation and three momentum equations in Cartesian coordinates through elimination of the pressure p by taking the curl of the momentum equations and subsequent introduction of the vorticity vector $\boldsymbol{\omega} = -\mathrm{rot}(u, v, w,)^T$ with its components ω_x, ω_y and ω_z. Fig. 2 gives an overview over the rectangular integration domain: Let x, y and z denote the axes in the leading edge normal, wall normal and spanwise direction and u, v and w the associated velocity components, respectively. The inflow velocity Q_∞ can then be decomposed into a leading edge normal component U_∞ and a leading edge parallel component W_∞ giving rise to a sweep angle

$$\Psi_\infty = \arctan\left(\frac{\bar{W}_\infty}{\bar{U}_\infty}\right) = \arctan(W_\infty) \tag{1}$$

with a bar used to distinguish dimensional quantities throughout the text. All quantities are calculated in a non-dimensional form based on the fixed chordwise inflow conditions consisting of $\bar{U}_\infty = 30$ m/s, a chordwise reference length $\bar{L} = 0.05$ m and

the kinematic viscosity $\bar{\nu} = 15 \cdot 10^{-6}$ m^2/s of air, resulting in a Reynolds number of $Re = 100\,000$. The quantities y, v, ω_x, ω_z are subjected to the $\sqrt{Re}$-stretching known from the boundary-layer equations in the code, but are displayed without it in the illustrations. The key assumption for infinite swept geometries is homogeneity ($\frac{\partial}{\partial z} \equiv 0$) in span for laminar calculations. The resulting set of equations consists of three vorticity transport equations

$$\frac{\partial \omega_x}{\partial t} + \frac{\partial (v\omega_x - u\omega_y)}{\partial y} = \frac{1}{Re}\frac{\partial^2 \omega_x}{\partial x^2} + \frac{\partial^2 \omega_x}{\partial y^2} \tag{2}$$

$$\frac{\partial \omega_y}{\partial t} - \frac{\partial (v\omega_x - u\omega_y)}{\partial x} = \frac{1}{Re}\frac{\partial^2 \omega_y}{\partial x^2} + \frac{\partial^2 \omega_y}{\partial y^2} \tag{3}$$

$$\frac{\partial \omega_z}{\partial t} + \frac{\partial (u\omega_z)}{\partial x} + \frac{\partial (v\omega_z)}{\partial y} = \frac{1}{Re}\frac{\partial^2 \omega_z}{\partial x^2} + \frac{\partial^2 \omega_z}{\partial y^2} \tag{4}$$

and the three Poisson equations for the velocity components

$$\frac{\partial^2 u}{\partial x^2} = -\frac{\partial^2 v}{\partial x \partial y} \tag{5}$$

$$\frac{1}{Re}\frac{\partial^2 v}{\partial x^2} + \frac{\partial^2 v}{\partial y^2} = -\frac{\partial \omega_z}{\partial x} \tag{6}$$

$$\frac{\partial^2 w}{\partial x^2} = \frac{\partial \omega_y}{\partial x} \tag{7}$$

In this quasi-three-dimensional set of Eqs. (5), (6) and (4) for u, v and ω_z are decoupled from the remaining ones. They remain unchanged with respect to the unswept case and can be solved a priory and independently from Eqs. (2), (3) and (7), which are only necessary to determine ω_x, ω_y and w in swept configurations. This decoupling is known as the *independence principle* of incompressible flow. The more common velocity–pressure formulation shows the same splitting, as w vanishes from the continuity equation and the x- and y-momentum equation. As a consequence u, v, p, ω_z and any quantity derived directly from them never depend on the sweep angle or the spanwise position, if an incompressible laminar flow is homogeneous in span and exhibits the same chordwise inflow conditions as the unswept base case. This implies that while

U_∞ stays constant, W_∞ has to be adjusted according to (1), so that Re_{Q_∞} based on the inflow velocity becomes a function of the sweep angle Ψ_∞ and the constant Re based on U_∞

$$Re_{Q_\infty} = \frac{\bar{Q}_\infty \cdot \bar{L}}{\bar{\nu}} = \sqrt{1 + \tan^2(\Psi_\infty)} Re \qquad (8)$$

3. Numerical considerations

The chosen DNS-algorithm has evolved over the years and was successfully applied to various transitional flows as for example described in Rist and Fasel [24], Bake, Meyer and Rist [2] or Wassermann and Kloker [28]. Typically it was utilised to provide a highly accurate, steady, laminar base flow for unsteady DNS-calculations of the disturbance propagation within this flow. For the scheme Eqs. (2)–(7) are discretized with central compact finite-differences of fourth order in x and y. The exact initial conditions within the flow field are not crucial. However, prescribing a solution with some resemblance to the expected end result will speed up convergence. For attached flows Falkner–Scan–Cooke-profiles as derived by Cooke [7] can be prescribed according to the local pressure gradient with matching vorticity profiles. As we are facing separated regions were no similarity solution exists, this is here only done at the inflow and the corresponding dimensionless solution is then rescaled within the flowfield to match the local free-stream velocities in x and z at the upper domain edge. The resulting flow field can then be interpreted as the disturbed realisation of the desired stationary solution. To reach it Eqs. (2)–(7) are integrated in pseudo-time until these disturbances have been convected out of the domain or dissipated. For the present calculations tolerances were chosen such that convergence to steady state was reached when the residual in v, ω_z and w between two pseudo time levels was smaller then 10^{-10}.

3.1. The DNS-algorithm and applied boundary conditions

For each time step the convection terms of Eqs. (2)–(4) are linearised by treating their components as 'lagging coefficients'. As we are seeking a stationary solution, accuracy in pseudo-time is less important then stability and a strongly dissipative behaviour in t. The decoupled transport equations are therefore integrated by a semi-implicit variant of the ADI-algorithm of Beam and Warming [4] in delta-formulation, which utilises the scheme 'Euler implicit' (also known as 'backward Euler method') for the x-derivatives and 'Euler explicit' (also known as 'forward Euler method') for those in y. Afterwards the linear equation system of the discretized v-Poisson equation (6) is solved iteratively by means of a Gauß–Seidel-Iteration with successive overrelaxation (LSORV). Finally, by applying a compact scheme of sixth order and Dirichlet conditions at both boundaries, the simplified u- and w-'Poisson' equations (5) and (7) can be directly integrated in x with negligible computational effort. Thus, effectively only three transport equations and one Poisson equation have to be solved just as in the velocity-pressure formulation.

The dominant elliptical character of the incompressible Navier–Stokes equations requires Dirichlet or von-Neumann boundary conditions for all flow quantities $q \in \{u, v, w, \omega_x, \omega_y, \omega_z\}$ at the boundaries: Falkner–Scan–Cooke profiles without pressure gradient are prescribed at the inflow boundary located at $x_o = 0.37$. At the impermeable wall no-slip conditions for the velocity components u_w, w_w as well as $v_w = 0$ and $\frac{\partial v_w}{\partial y} = 0$ are employed, while special equations

$$\frac{\partial \omega_{x,w}}{\partial x} = -\frac{\partial \omega_{y,w}}{\partial y}, \quad \omega_{y,w} = 0, \quad \frac{\partial \omega_{z,w}}{\partial x} = -\frac{\partial^2 v_w}{\partial y^2}$$

were derived for the vorticity components. At the outflow $x_N = 5.05$, approximately eight separation bubble lengths downstream

of the reattachment line at $x_{sep} = 2.13$, an attached boundary layer flow has redeveloped. For these flows second x-derivatives are small in accordance with the boundary layer theory, so that these terms can be neglected locally for $q_N \in \{v_N, \omega_{x,N}, \omega_{y,N}, \omega_{z,N}\}$ at the outflow boundary. However, as (5) and (7) rely on exactly these terms, the relations

$$\frac{\partial^2 u_N}{\partial y^2} = \frac{\partial \omega_{z,N}}{\partial y}, \quad \frac{\partial^2 w_N}{\partial y^2} = \frac{1}{Re}\frac{\partial \omega_{y,N}}{\partial x} - \frac{\partial \omega_{x,N}}{\partial y}$$

are applied for the calculation of u and w. In potential flow the vorticity vanishes, so $\omega_{x,e} = \omega_{y,e} = \omega_{z,e} = 0$ are prescribed at the upper edge of the integration domain at $y_e = 0.059$, which amounts to 18 displacement thicknesses at the inflow. A direct application of the continuity equation yields $\frac{\partial v_e}{\partial y} = -\frac{\partial u_e}{\partial x}$. The upper boundary conditions for the free-stream velocity components u_e and w_e are decisive, because they determine all the properties of the resulting separation bubble: With the choice of the $u_e(x)$-distribution the local pressure gradient is implicitly prescribed via the Bernoulli equation. Here the distribution displayed in Fig. 2 remains on the inflow level until $x_1 = 0.706$. To enforce the boundary layer separation at $x_{sep} = 1.75$ this part is followed by a smooth decrease of 8.95% until $x_2 = 2.42$, whereupon it stays constant again to allow for laminar reattachment. Different sweep angles may be realised by varying $W_\infty = \tan(\Psi_\infty)$, which globally determines the spanwise free-stream velocity $w_e = W_\infty$.

3.2. Validation of the DNS-algorithm

Oswatitsch [22] has given an analytical solution of the incompressible Navier–Stokes equations in the neighbourhood of a separation point for a two-dimensional, laminar boundary layer. It allows a calculation of the separation angle

$$\tan(\varphi_{sep}) = -3\left(\frac{\frac{\partial \tau_x}{\partial x}}{\frac{\partial p}{\partial x}}\right)\bigg|_{x=x_{sep},\, y=0} \qquad (9)$$

from the wall shear stress component τ_x in x-direction and the wall pressure, both evaluated at the point of separation. Van Ingen convincingly confirmed the validity of this formula experimentally in [16]. The comparison in Fig. 3(a) of $\varphi_{sep} = 1.39°$ calculated from (9) to the dividing streamline Ψ_o of the separation bubble shows excellent agreement in the neighbourhood of the separation position $x_{sep} = 1.75$.

Additionally, the step-size dependence of the numerical solution was investigated by grid refinement studies for the case $\Psi_\infty = 45°$. The standard resolution of 1394×97 grid points in x- and y-direction with $\Delta x = 3.36 \cdot 10^{-3}$ and $\Delta y = 6.2 \cdot 10^{-4}$ was independently halved and doubled. The maximum relative error

$$\text{error}_{rel\,max} := \frac{\max_{x,y} |q_{fine}(x,y) - q_{coarse}(x,y)|}{\max_{x,y} |q_{fine}(x,y)|}$$

was then determined for all flow quantities $q \in \{u, v, w, \omega_x, \omega_y, \omega_z\}$ separately. As the maximum deviation of the coarse solution to the fine one was only 0.017% for a variation of the stepsize in x, the standard x-resolution was found to be finer than necessary. The maximum global error for a variation of the stepsize in y occurred in v and is shown in Fig. 3(b). Clearly, the coarse resolution of only 49 grid points in y would have been insufficient. But the maximum deviation of the standard resolution compared to the fine one is still 0.07% and only visible in an enlarged cutout of Fig. 3(b). Simple profiles like Fig. 4 are based on the standard, more sophisticated visualisations as Fig. 3(a) or 5 on the fine grid in y both with the standard resolution in x. It follows that the spatial resolution of the DNS is good.

Note that transitional flows are much more demanding in terms of spatial resolution. Therefore, to accurately calculate the disturbance propagation in the unsteady laminar separation bubbles
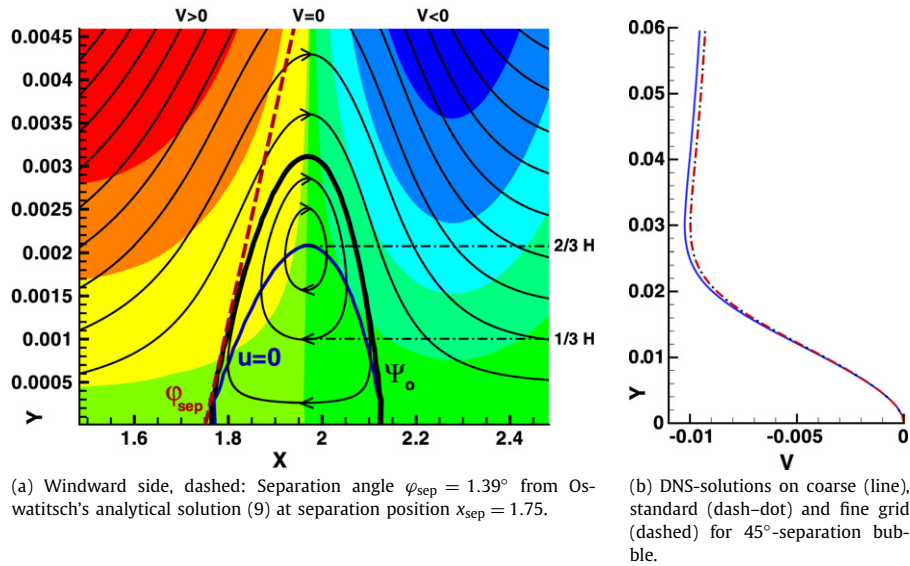
(a) Windward side, dashed: Separation angle $\varphi_{sep} = 1.39°$ from Oswatitsch's analytical solution (9) at separation position $x_{sep} = 1.75$.

(b) DNS-solutions on coarse (line), standard (dash–dot) and fine grid (dashed) for 45°-separation bubble.

Fig. 3. Code validation. Left: Separation angle compared to sweep angle independent cross-section of present 45°-bubble with coloured v-iso-levels, internal and external u–v-streamlines and dividing streamline Ψ_o. Centre of circulation inside: Intersection of isolines $u = 0$ and $v = 0$. Ratio of height $H = 0.0031$ to length $L = 0.38$ as 1 : 120. Right: Test for y-step size independence of presented separation bubble series. Solution on standard grid (97 y-points, dash–dot) compared to coarse (line, 49 points) and fine grid (dashed, 201 points), all with 1394 points in x. Displayed is the v-profile at $x = 2.21$ where maximum global error occurs. The standard and the fine solution are nearly indistinguishable.

(a) w-profiles for all sweep angles show the global upper boundary condition $w_e = \tan(\Psi_\infty)$.

(b) All w-profiles for $\Psi_\infty > 0$ coincide with the generic 45°-profile, if normalised by $\tan(\Psi_\infty)$.

(c) Corresponding crossflow profiles w_s at the separation position $x_{sep} = 1.75$.

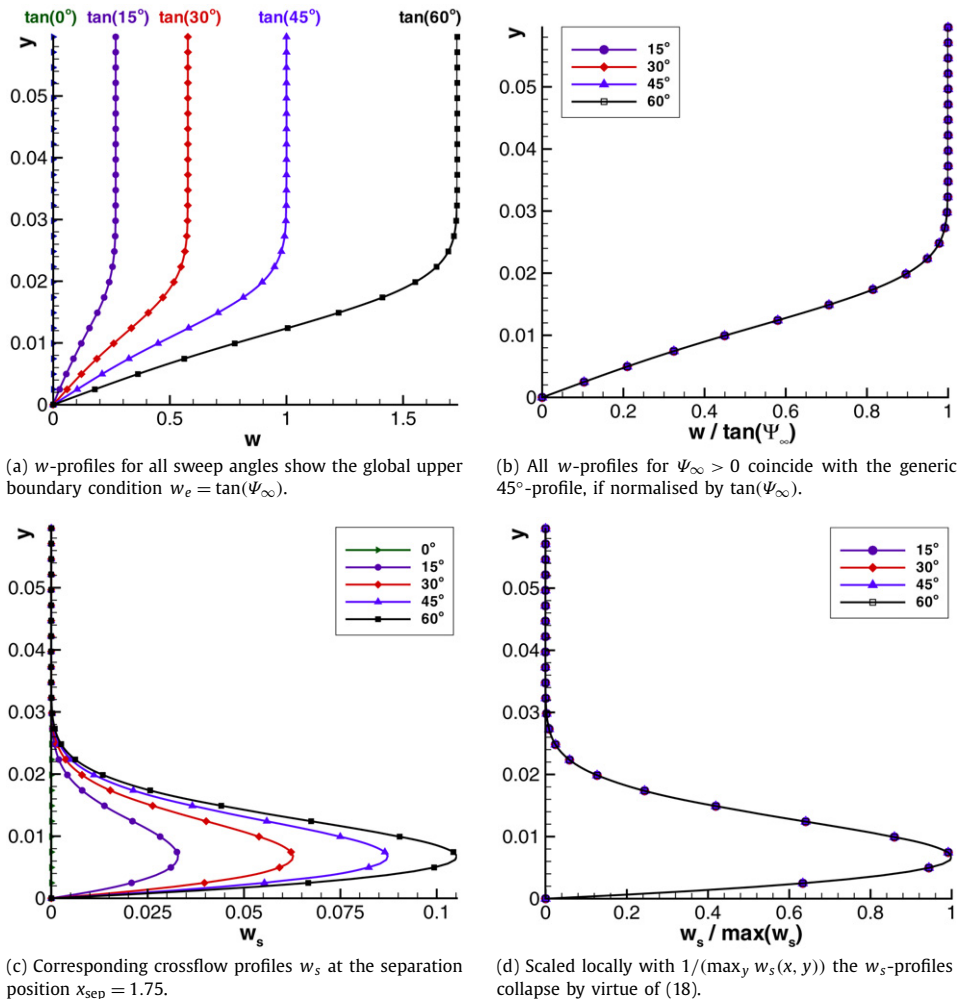(d) Scaled locally with $1/(\max_y w_s(x, y))$ the w_s-profiles collapse by virtue of (18).

Fig. 4. Spanwise velocity profiles $w(y)$ and crossflow profiles $w_s(y)$ at the separation position $x_{sep} = 1.75$ for the sweep angles of $\Psi_\infty = 0°, 15°, 30°, 45°$ and $60°$. For a given configuration the shape of the w-profiles is sweep angle independent. Every new sweep angle globally scales this generic 45°-solution by the spanwise free-stream velocity $w_e = \tan(\Psi_\infty)$. The derivation of the sweep angle independence of the shape of the crossflow profiles on the other hand requires local scaling.

published in Hetsch and Rist [11,12] the underlying base flows had to be resolved with twice to four times the standard resolution in x and y utilised here.

4. The influence of sweep on the general structure of swept laminar separation bubbles

4.1. The influence of sweep on the laminar flow quantities and resulting scaling laws

We are interested in the question how a given unswept laminar solution changes when a sweep angle Ψ_∞ is introduced. Clearly the flow quantities u, v, p and ω_z remain unchanged by virtue of the independence principle. Once the spanwise velocity component w is determined with an appropriate method, the vorticities

$$\omega_x = -\frac{\partial w}{\partial y}, \qquad \omega_y = \frac{\partial w}{\partial x} \tag{10}$$

can readily be obtained as derivatives of w, as the definition of the vorticity vector is simplified by the homogeneity in span.

Therefore, only the influence of the sweep angle on the key quantity w has to be analysed: As the velocities u and v are known a priori from the unswept solution, the z-momentum equation

$$\frac{\partial w}{\partial t} + u\frac{\partial w}{\partial x} + v\frac{\partial w}{\partial y} = \frac{1}{Re}\frac{\partial^2 w}{\partial x^2} + \frac{\partial^2 w}{\partial y^2} \tag{11}$$

becomes linear in w and allows for linear superposition of solutions, if this is compatible with the boundary conditions. Let a subscript 'e' denote any quantity at the upper boundary of the computational domain in the potential free-stream. The no-slip condition $w(0) = 0$ at the wall is homogeneous and the upper boundary condition a global constant, as the vorticities $\omega_{y,e} = \frac{\partial w_e}{\partial x}$ and $\omega_{x,e} = -\frac{\partial w_e}{\partial y}$ must vanish in potential flow and the geometry implies $\frac{\partial w}{\partial z} = 0$. This constant can be determined at the inflow, where $w_e = W_\infty = \tan\Psi_\infty$ by definition of the sweep angle (1). Therefore, spanwise velocity profiles for an arbitrary sweep angle $0 < \Psi_\infty < 90°$ must coincide after normalisation with the global scaling factor $1/\tan(\Psi_\infty)$ as demonstrated by Figs. 4(a) and 4(b). This scaling property of w is automatically transfered to ω_x and ω_y, because differentiation is a linear operation. Thus, after the normalisation of w, ω_x and ω_y the profiles of *all* flow quantities coincide with the generic 45°-case, which is the only one to remain unchanged as $\tan(45°) = 1$. This leads to the important scaling property that the *exact* laminar flow field for any desired sweep angle $0 \leqslant \Psi_\infty < 90°$ may be analytically obtained from any given swept solution for a sweep angle $0 < \widetilde{\Psi}_\infty < 90°$ by scaling via

$$u = u_{\widetilde{\Psi}_\infty}, \quad v = v_{\widetilde{\Psi}_\infty}, \quad \omega_z = \omega_{z,\widetilde{\Psi}_\infty}$$
$$w = \frac{\tan(\Psi_\infty)}{\tan(\widetilde{\Psi}_\infty)} w_{\widetilde{\Psi}_\infty}, \quad \omega_x = \frac{\tan(\Psi_\infty)}{\tan(\widetilde{\Psi}_\infty)} \omega_{x,\widetilde{\Psi}_\infty}$$
$$\omega_y = \frac{\tan(\Psi_\infty)}{\tan(\widetilde{\Psi}_\infty)} \omega_{y,\widetilde{\Psi}_\infty} \tag{12}$$

It follows that a known swept laminar solution from the literature can be used to reconstruct the corresponding flow for any other sweep angle *a posteriori* in swept infinite configurations.

In swept configurations a transformation of the flow field into a streamline-oriented coordinate system is often of particular interest. By definition the streamwise velocity component u_s and the crossflow w_s

$$u_s := \cos(\Psi_e) \cdot u + \sin(\Psi_e) \cdot w \tag{13}$$

$$w_s := -\sin(\Psi_e) \cdot u + \cos(\Psi_e) \cdot w \tag{14}$$

are tangential and normal to the local direction

$$\Psi_e(x) = \arctan\big(W_\infty / u_e(x)\big)$$

of the potential streamline. In order to investigate how sweep effects them, let a double-bar superscript denote any sweep angle independent quantity:

$$u = \bar{\bar{u}}, \quad w = \tan(\Psi_\infty)\bar{\bar{w}}_{45°}, \quad \Psi_e = \arctan\big(\tan(\Psi_\infty)/\bar{\bar{u}}_e\big) \tag{15}$$

It follows from (1) and the discussion above that Eqs. (13) and (14) become:

$$u_s = \cos\left[\arctan\left(\frac{\tan(\Psi_\infty)}{\bar{\bar{u}}_e}\right)\right]\bar{\bar{u}}$$
$$\quad + \sin\left[\arctan\left(\frac{\tan(\Psi_\infty)}{\bar{\bar{u}}_e}\right)\right]\tan(\Psi_\infty)\bar{\bar{w}}_{45°}$$
$$w_s = -\sin\left[\arctan\left(\frac{\tan(\Psi_\infty)}{\bar{\bar{u}}_e}\right)\right]\bar{\bar{u}}$$
$$\quad + \cos\left[\arctan\left(\frac{\tan(\Psi_\infty)}{\bar{\bar{u}}_e}\right)\right]\tan(\Psi_\infty)\bar{\bar{w}}_{45°}$$

Therefore, in general no *global* scaling results in collapsing u_s or w_s-profiles for different sweep angles. For the special case of $\bar{\bar{u}}_e \equiv 1$ however the equations simplify to

$$\bar{\bar{u}}_e \equiv 1 \implies u_s = \cos(\Psi_\infty) \cdot \{\bar{\bar{u}} + \tan^2(\Psi_\infty)\bar{\bar{w}}_{45°}\} \tag{16}$$
$$w_s = \sin(\Psi_\infty) \cdot \{\bar{\bar{w}}_{45°} - \bar{\bar{u}}\} \tag{17}$$

As the free-stream pressure distribution expresses itself in the u_e-distribution via the Bernoulli equation, this means that the cross-flow velocity w_s can be normalised globally with the scaling factor $1/\sin(\Psi_\infty)$ for swept, zero-pressure gradient flows. Pressure gradients imply curved potential streamlines, so that in general (16) and (17) may be used as an approximation in regions with relatively straight potential streamlines, where the local free-stream direction Ψ_e remains close to Ψ_∞.

By considering *local* scaling laws[1] on the other hand, at least the shape of the crossflow profile w_s can be shown to be sweep angle independent in general. This is achievable with the help of the local free-stream velocity $u_{s,e}$:

$$\frac{w_s}{u_{s,e}} = \sin(\Psi_e)\cos(\Psi_e)\left(\frac{w}{W_\infty} - \frac{\bar{\bar{u}}}{\bar{\bar{u}}_e}\right) \tag{18}$$

The sweep angle independence follows immediately from $w/W_\infty = \bar{\bar{w}}_{45°}$ and can be exploited for example in the form $w_s/(\max_y w_s(x, y))$, as demonstrated by Figs. 4(c) and 4(d). As $\bar{\bar{u}}_e \approx 1$ throughout the given base flow, a global scaling with $1/\sin(\Psi_\infty)$ produces basically the same collapse by virtue of (17).

4.2. An improved solution strategy on the basis of the independence principle

Especially for a series of flow calculations with a common pressure distribution yet different sweep angles, the scaling laws of Section 4.1 allow for a considerable simplification. This general strategy is *not* restricted to separation bubbles, the vorticity–velocity formulation or a particular DNS-algorithm, but applicable to any stationary incompressible flow where the independence principle holds:

(i) Solve the unswept case for u, v and ω_z (or p, depending on the formulation).

---

[1] The authors are indebted to the referee, who kindly provided scaling law (18). To the best of his knowledge it has not been published before.

(ii) Solve the z-momentum equation (11) for w for the generic 45°-case.

(iii) Calculate ω_x and ω_y for $\Psi_\infty = 45°$ from (10) as derivatives of w.

(iv) Obtain flow field for any desired sweep angle by global scaling of w, ω_x, ω_y with $\tan(\Psi_\infty)$.

For the present study the z-momentum equation (11) has been recast in the form

$$\frac{\partial w}{\partial t} = -R_w, \quad R_w = \frac{\partial(uw)}{\partial x} + \frac{\partial(vw)}{\partial y} - \frac{1}{Re}\frac{\partial^2 w}{\partial x^2} - \frac{\partial^2 w}{\partial y^2} \quad (19)$$

with a space operator R_w, which was discretized as in Section 3.1. The time integration of (19) was performed with a predictor–corrector approach utilising a third-order Adam–Bashforth scheme corrected by the trapezoid rule. As expected from the independence principle, independent calculations according to the original algorithm from Section 3.1 were identical to scaled base flows of the 45°-solution of the explicit scheme within the computational accuracy of $\mathcal{O}(10^{-10})$. All visualisations shown in the paper are based on previous calculations which still utilised the original algorithm of Section 3.1.

For a demanding 45°-baseflow (four times the domain height of the current study, 2786×1537 grid points in x and y) the original algorithm needed 53 h user-time on a single CPU of a NEC-SX5 for a residual of 10^{-10} in all six flow quantities. With the new approach 24 h had to be spent for a converged solution of the unswept problem. With u and v already converged the solution of (11) converges faster and was obtained in 13 h. Thus, the new approach took 37 h for the three-dimensional flow field and was 30% faster. But most importantly an arbitrary number of flow fields with different sweep angles could be immediately obtained afterwards simply by scaling.

4.3. The general structure of swept laminar separation bubbles

The independence principle and the resulting scaling laws of Section 4.1 allow us to link the main topological features of laminar separation bubbles in swept infinite geometries to their unswept counterparts.

4.3.1. Similarities to unswept laminar separation bubbles

With u, v, p and ω_z the entire cross-section of a swept separation bubble remains unaffected by a rising sweep angle. Therefore, the cross-section of the present 45°-separation bubble in Fig. 3(a) is identical to the one of the corresponding unswept case, which immediately determines the sense of rotation for arbitrary sweep angles. The slow backflow observed in the lower two-thirds of the bubble must be balanced by a slightly stronger movement in the direction of the outer flow above the isoline $u = 0$. This is required by mass conservation, because in the unswept case the spanwise velocity w vanishes and no fluid can pass the dividing streamline

$$\Psi_o = \big\{(x, y) \mid \Psi(x, y) = 0\big\}, \quad \text{with } \Psi(x, y) = \int_0^y u(x, \tilde{y}) \, d\tilde{y} \quad (20)$$

Likewise, no fluid can pass the corresponding separation stream surface visualised in Fig. 5 in the swept case. Fluid inside the separation bubble is therefore 'trapped' and simply circulates in the case of vanishing sweep.

Furthermore, the homogeneity in span enforces leading edge-parallel separation and reattachment lines, so that separation remains a two-dimensional phenomenon in the x–y-plane for arbitrary sweep angles $\Psi_\infty < 90°$. The sweep angle independence of the leading edge normal component of the wall shear stress
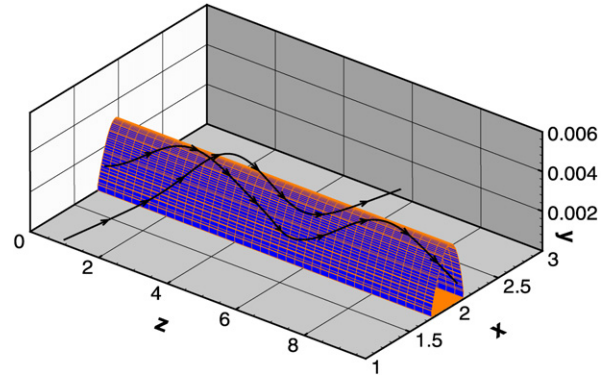

Fig. 5. Internal and external streamlines of the 30°-laminar separation bubble. Due to homogeneity in span its surface can be obtained from the dividing streamline Ψ_o from (20) for arbitrary cross-sections. Helical, anti-clockwise motion inside (viewed in direction of spanwise flow). External streamlines displace faster fluid layers upwards while gliding over the bubble.

$\tau_x = \mu(\frac{\partial u}{\partial y})|_w$ implies the occurrence of separation and reattachment at the same x-position as in the unswept case, marked by a sign change in τ_x. Note that the symmetrical, elliptical shape of the separation bubble in Fig. 3(a) is a consequence of the assumed quiet inflow conditions modelled by an absence of any disturbances. As demonstrated by Rist [23] for the mean flow of the unswept and by Hetsch and Rist [12] for the swept case, the typical asymmetrical outline with a hump at its rearward end, known from visualisations of transitional separation bubbles, develops under the presence of unsteady disturbances which trigger vortex shedding.

4.3.2. Differences to unswept laminar separation bubbles

Differences to the unswept case become manifest in the spanwise velocity component w in accordance with the analysis of Section 4.1. The three-dimensional velocity field of a swept bubble consists of a sweep angle independent two-dimensional u–v-cross-section which is merely *superimposed* with w. With increasing sweep angle this spanwise component grows in magnitude like $\tan(\Psi_\infty)$, but its shape, the normalised x–y-distribution of w, is again sweep angle independent and fixed by the generic 45°-solution. Inside a swept separation bubble w forces the closed streamlines of the unswept case into the helical motion displayed in Fig. 5. Its existence gives rise to a spanwise wall shear stress $\tau_z := \mu(\frac{\partial w}{\partial y})|_w$. In accordance with Davis, Carter and Reshotko [8] τ_z was found to be positive throughout the flow field, as there is no flow reversal in the spanwise direction. Thus, the total wall shear stress $\tau_w = \tau_x + \tau_z$ is non-zero at separation and additionally does not show its minimum there, but inside the bubble, which makes it hard to determine the exact separation position of swept separation bubbles experimentally by measuring wall shear stresses.

5. Summary and conclusions

The general structure of separation bubbles in strictly laminar flow fields on swept infinite geometries has been investigated by means of an analysis of the incompressible Navier–Stokes equations and direct numerical simulations of short laminar separation bubbles. The applicability of the independence principle for incompressible laminar flow enforces an unique topology which includes unswept configurations as a special case: Laminar separation bubbles form leading edge parallel stream tubes with a spanwise outflow and a helical motion inside as depictured in Fig. 5. As long as the chordwise inflow conditions are kept constant, the cross-section of the bubble is sweep angle independent, so that in par-

ticular the separation and reattachment position coincide with the corresponding unswept case.

Interestingly, exactly the same topological features as in Fig. 5 have been observed experimentally by Horton [15] for series of transitional separation bubbles on a flat plate with displacement body, an experimental approximation of a swept infinite wing, for a fixed sweep angle of 26.5°. The independence principle could potentially provide a link between both observations and thus explain the obvious qualitative agreement of the investigated separation bubbles in different flow regimes: Based on an evaluation of the rare literature on swept separation bubbles known to us, we strongly suspect that the independence principle is extendable in good approximation to the *mean* flow of transitional separation bubbles up to sweep angles that are significant for practical applications. Within the scope of the literature cited in the introduction, the authors of the corresponding articles independently report the independence of chordwise flow properties up to sweep angle of about 40° and repeatedly affirmed the applicability of the independence principle in their particular configuration. If this could be proven in general, the topology first described by Horton and analysed here in detail on the basis of the independence principle would be the only possible structure of the mean flow of separation bubbles in swept infinite geometries, as long as the independence principle holds. It should be noticed though, that due to the lack of literature our survey had to rely strongly on results of backward-facing-step flows, which do not include curvature effects and exhibit a fixation of the separation position as opposed to the situation on swept infinite wings.

An analysis of the incompressible Navier–Stokes equations also yielded general scaling laws for laminar flows with a homogeneous spanwise direction such as the flow over a swept infinite flat plate subjected to a pressure gradient. If the leading edge-normal inflow conditions are held constant, flow quantities already present in the unswept case are sweep angle independent. So is the *shape* of any quantity which additionally appears in swept flows, because their distributions in the x–y-plane are fixed by the generic 45°-solution, for which the general scaling law (12) takes its simplest form. A rising sweep angle Ψ_∞ merely scales their amplitudes with the global factor $\tan(\Psi_\infty)$. As the tan-function is strictly monotonous, it follows that the locations of local or global extrema of the basic flow quantities within the flow field are also sweep angle independent. Furthermore, in zero-pressure-gradient flows the crossflow w_s scales with a global factor of $\sin(\Psi_\infty)$. This remains approximately true in regions where the potential streamlines are essentially straight and remain close to the direction of the sweep angle.

The scaling law (12) allows an exact reconstruction of the laminar flow field for arbitrary sweep angles $0° \leqslant \Psi_\infty < 90°$ from any known swept solution of the same configuration. A general strategy for efficient DNS-calculations of series of swept cases based on them is outlined in Section 4.2. As a direct consequence of the independence principle of the incompressible Navier–Stokes equations these results do not depend on the presence of separation bubbles in the flow field. They may be useful for the analysis of newly obtained results, for code validation purposes or for the extrapolation of results available from the literature to different sweep angles.

Acknowledgements

References

[1] M. Alam, N.D. Sandham, Direct numerical simulation of 'short' laminar separation bubbles with turbulent reattachment, J. Fluid Mech. 403 (2000) 223–250.

[2] S. Bake, D.G.W. Meyer, U. Rist, Turbulence mechanisms in Klebanoff transition: A quantitative comparison of experiment and direct numerical simulation, J. Fluid Mech. 459 (2002) 217–243.

[3] F. Bao, Experimental investigations of transitional unsteady separated vortex flows, PhD thesis, Faculty of Mechanical Engineering, Universität Hannover, Germany, 2001. Also published as DLR-report 2001-20.

[4] R.M. Beam, R.F. Warming, An implicit factored scheme for the compressible Navier–Stokes equations, AIAA J. 16 (4) (1978) 393–402.

[5] W.R. Briley, A numerical study of laminar separation bubbles using the Navier–Stokes equations, J. Fluid Mech. 47 (1971) 713–736.

[6] F.D. Barkey-Wolfe, Swept and unswept separation bubbles, PhD thesis, Pembroke College, Cambridge, UK, 1987.

[7] J.J.C. Cooke, The boundary layer of a class of infinite yawed cylinders, Proc. Camb. Phil. Soc. 46 (1950) 645–648.

[8] R. Davis, J. Carter, E. Reshotko, Analysis of transitional separation bubbles on infinite swept wings, AIAA J. 25 (3) (1987) 421–428.

[9] E. Greff, In-flight measurements of static pressures and boundary-layer state with integrated sensors, J. Aircraft 28 (5) (1991) 289–299.

[10] A.H. Herbst, D.S. Henningson, The influence of periodic excitation on a turbulent separation bubble, Flow Turbulence Combustion 76 (2006) 1–21.

[11] T. Hetsch, U. Rist, The effect of sweep on laminar separation bubbles, in: R. Govindarajan (Ed.), Sixth IUTAM Symposium on Laminar–Turbulent Transition, Proc. IUTAM-Symp., Bangalore, India, December 2004, in: Fluid Mechanics and its Applications, vol. 78, Springer, 2006, pp. 395–400.

[12] T. Hetsch, U. Rist, Direct numerical simulation and analysis of the flow field around a swept laminar separation bubble, in: W. Nagel, W. Jäger, M. Resch (Eds.), High Performance Computing in Science and Engineering '06, Springer, 2007, pp. 205–221.

[13] T. Hetsch, U. Rist, Accuracy of local and nonlocal linear stability theory in swept laminar separation bubbles, AIAA J. (2009) doi:10.2514/1.37997.

[14] T. Hetsch, U. Rist, The influence of sweep on the linear stability of a series of swept laminar separation bubbles, Eur. J. Mech. B/Fluids 28 (4) (2009) 494–505.

[15] H. Horton, Laminar separation bubbles in two and three dimensional incompressible flow, PhD thesis, Department of Aeronautical Engineering, Queen Mary College, University of London, UK, 1968.

[16] J.L. van Ingen, On the calculation of laminar separation bubbles in two-dimensional incompressible flow, AGARD CP 168 (1977) 11-1–11-16.

[17] L.E. Jones, R.D. Sandberg, N.D. Sandham, Direct numerical simulations of forced and unforced separation bubbles on an airfoil at incidence, J. Fluid Mech. 602 (2008) 175–207.

[18] W. Jürgens, H.-J. Kaltenbach, Eigenmode decomposition of turbulent velocity fields behind a swept, backward-facing step, J. Turbulence 4 (18) (2003) 1–21.

[19] H.-J. Kaltenbach, The effect of sweep-angle variation on the turbulence structure in a separated, three-dimensional flow, Theoret. Comput. Fluid Dynamics 16 (2003) 187–210.

[20] H.-J. Kaltenbach, G. Janke, Direct numerical simulation of a flow separation behind a swept, rearward-facing step at $Re_H = 3000$, Phys. Fluids 12 (9) (2000) 2320–2337.

[21] O. Marxen, M. Lang, S. Wagner, A combined experimental/numerical study of unsteady phenomena in a laminar separation bubble, Flow Turbulence Combustion 71 (2003) 133–146.

[22] L. Prandtl, K. Oswatitsch, K. Wieghardt, Führer durch die Strönungslehre, 9th edition, Vieweg, 1990.

[23] U. Rist, Zur Instabilität und Transition laminarer Ablöseblasen, Habilitation, University of Stuttgart, Germany, Shaker, 1999.

[24] U. Rist, H.F. Fasel, Direct numerical simulation of controlled transition in a flat-plate boundary layer, J. Fluid Mech. 298 (1995) 211–248.

[25] G. Selby, Applicability of the independence principle to subsonic turbulent flow over a swept rearward-facing step, AIAA J. 21 (1983) 1603–1604 (technical note).

[26] P.R. Spalart, G.N. Coleman, Numerical study of a separation bubble with heat transfer, Eur. J. Mech. B/Fluids 16 (2) (1997) 169–189.

[27] P.R. Spalart, M. Strelets, Mechanisms of transition and heat transfer in a separation bubble, J. Fluid Mech. 403 (2000) 329–349.

[28] P. Wassermann, M. Kloker, Mechanisms and passive control of crossflow-vortex-induced transition in a three-dimensional boundary layer, J. Fluid Mech. 456 (2002) 49–84.

[29] A.D. Young, H.P. Horton, Some results of investigations of separation bubbles, AGARD CP 4 (1966) 780–811.